Visualization of *Aspergillus fumigatus* biofilms with Scanning Electron Microscopy and Variable Pressure-Scanning Electron Microscopy: a comparison of processing techniques.

Lydia-Marie Joubert[1*], Jose AG Ferreira[2,3†], David A Stevens[2,3], Hasan Nazik[2,3], Kent L McDonald[5], Lynette Cegelski[4]

[1.] Cell Sciences Imaging Facility, Stanford University School of Medicine, Stanford CA, USA.
[2.] Division of Infectious Diseases and Geographic Medicine, Stanford University, Stanford CA, USA
[3.] California Institute for Medical research, San Jose CA, USA
[4.] Department of Chemistry, Stanford University, Stanford CA, USA
[5.] Electron Microscope Lab, 26 Giannini Hall MC 3330, University of California, Berkeley CA, USA

*Corresponding author: Lydia-Marie Joubert, lydiaj@stanford.edu.

Abstract: Aspergillus fumigatus biofilms consist of a three-dimensional network of cellular hyphae and extracellular matrix. They are involved in infections of immune-compromised individuals, particularly those with cystic fibrosis. These structures are associated with persistence of infection, resistance to host immunity, and antimicrobial resistance. Thorough understanding of structure and function is imperative in the design of therapeutic drugs. Optimization of processing parameters for an ultrastructural approach to understanding these structures was undertaken, to improve interpretation of electron microscopy results from cellular and extracellular biofilm components. Conventional and Variable Pressure Scanning Electron Microscopy were applied to analyze the structure of biofilms attached to plastic and formed at an air-liquid interface.

Keywords: Aspergillus fumigatus, biofilms, scanning electron microscopy, Variable Pressure-SEM, processing techniques.

† Current address: School of Medicine, Faculdade da Saúde e Ecologia Humana-FASEH, Vespasiano, Brazil

27 *Abbreviations:* BSE, Backscattered Electron; CF, cystic fibrosis; CPD, critical point drying; ECM,
28 extracellular matrix; EPS, extracellular polymeric substances; ET, Everhart-Thornley; FESEM,
29 Field Emission Scanning Electron Microscopy; GA, Glutaraldehyde; HMDS,
30 hexamethyldisilazane; NMR, Nuclear Magnetic Resonance; OsO4, osmiumtetroxide; PBS,
31 phosphate-buffered saline; PFA, paraformaldehyde; SE, Secondary Electron; SEM, Scanning
32 Electron Microscopy; SNR, Signal to Noise Ration; VP-SEM, Variable Pressure-SEM

33

34 *1.Introduction:*

35 A biofilm can be defined as a community of microbial cells surrounded by a self-produced
36 polymeric matrix, which facilitates adhesion among cells and/or to other surfaces or interfaces
37 (Costerton et al., 1995; Lappin-Scott et al., 2014; Donlan, 2002). *Aspergillus fumigatus* has
38 recently been shown to form three-dimensional assemblies, 10-200μm thick, and with typical
39 biofilm characteristics (Muller 2011; Beauvais et al., 2007, 2009, 2014; Kaur and Singh 2014;
40 Mowat et al., 2007). *A. fumigatus* is frequently isolated from cystic fibrosis (CF) patients, and
41 *Aspergillus* biofilms contribute to virulence in CF and invasive pulmonary aspergillosis (Speirs
42 et al., 2012; Vrankrijker et al., 2011). *A. fumigatus* biofilms are of increasing biomedical interest
43 due to their association with chronic and lethal infections, notably in immunosuppressed
44 patients, and their increased resistance to antifungal agents (Santos et al., 2015). Fungal
45 biofilms also colonize abiotic surfaces and contribute to biofilm-related infections of implanted
46 medical devices, e.g. catheters, pacemakers, prosthetic devices, and lenses (Nobile and Johnson,
47 2015; Youysif et al., 2015, Kojic and Darouiche, 2004). An estimated 80% of all infections in the
48 USA are associated with microbial biofilms (Fox and Nobile, 2012). Biofilms are a significant
49 cause of morbidity and mortality in the clinic and additionally impacts the health care system
50 through escalating costs of treating chronic biofilm-associated infections.

51 Understanding the composition and ultrastructure of microbial biofilms is imperative in
52 understanding function and to developing strategies to control biofilm formation. The
53 extracellular matrix (ECM) includes the extracellular polymeric substances (EPS) that surround
54 resident cells, and serves as a physical and chemical barrier to antimicrobials, competitors and
55 immune responses (Manavuthu et al., 2014; Xiao et al., 2012). The ECM also contributes to

56 biofilm hydration and nutrient transport (Flemming et al., 2007), and provides the mechanical
57 integrity to withstand turbulent fluid forces and retain biofilm structure. Biofilms can be multi-
58 species and can change over time, where the biofilm can accumulate 'immigrant' microbes,
59 altering the structure and function of the community. Characterization of the biofilm
60 extracellular matrix, in addition to its cellular organization, is therefore important for a holistic
61 analysis of biofilm structure-function relationships.

62 It has been shown *in vitro* that *Aspergillus* produces an extracellular matrix (ECM) with typical
63 biofilm characteristics under static and shaken, submerged conditions (Muller et al., 2011). In a
64 recent study, we implemented a top-down approach to examine the composition and
65 architecture of the ECM produced by *A. fumigatus* (Reichhardt et al., 2015) using solid-state
66 Nuclear Magnetic Resonance (NMR) and Scanning Electron Microscopy (SEM). The top-down
67 NMR approach was used to measure and quantify fundamental chemical parameters of the
68 intact ECM. The NMR analysis determined that the ECM of *A. fumigatus* biofilms grown in RPMI
69 1640 nutrient medium was composed of predominantly polysaccharide and proteins,
70 accounting for ~80% of the ECM, with lipids and aromatic compounds contributing to the
71 remaining 20%. NMR is a powerful tool in the analysis of ECM chemical composition (Cegelski,
72 2015; Reichhardt et al., 2016). Yet, SEM is uniquely suited to the analysis of biofilm architecture
73 and ultrastructure. SEM analysis of the biofilm samples in the NMR study showed biofilm
74 hyphae as being densely packed and surrounded by tightly woven webs of ECM, with some
75 ECM serving to glue hyphae together into a contiguous network.

76 In the present work, we report on the development of optimal protocols for examining *A.*
77 *fumigatus* biofilms by SEM and the new details that are observed using SEM. Electron
78 microscopy generally introduces some artifacts in structure, and interpretation of
79 ultrastructure includes cognition of the physico-chemical influence of each step of processing
80 protocols. The protocol of choice is therefore mostly optimized for a specific feature that is
81 under investigation (Bozzolla and Russell, 1999; Joubert et al., 2015). Stabilization of proteins
82 through aldehyde cross-linking, with post-fixation of lipids via osmiumtetroxide (OsO_4),
83 generally maintain ultrastructure (Hayat, 2000; Bozzolla and Russell, 1999), while preservation
84 of fine features is attempted through critical point drying (CPD) or hexamethyldisilazane
85 (HMDS) as a final drying agent (Bray et al., 1993). In biofilms, some loss of 3D architecture is

86 commonly associated with dehydration required for conventional SEM (Alhede et al., 2012).
87 Variable Pressure (VP)-SEM enables the observation of biofilms in their natural hydrated state
88 (Weimer et al., 2005; Priester et al., 2007; Weber et al., 2014), with the ECM often observed as a
89 gel-like film. However, resolution is compromised under extended pressures and through the
90 inclusion of water vapor and gas in the specimen chamber; cellular features are hidden under
91 the electron-dense film, which may blanket hydrated cells. Ruthenium Red has been described
92 as a suitable contrasting agent in hydrated biofilms (Priester et al., 2007, Weber et al., 2014),
93 and recently ionic liquids (IL) have been reported to improve imaging of hydrated biofilms by
94 preserving their natural in situ 3D architecture (Asahi et al., 2015, Joubert and McDonald,
95 2016). OsO_4 has also been described as a contrasting agent to localize cells growing on
96 hydrogels, by providing differential binding to lipids, which are generally located in cell
97 membranes and cellular compartments (Joubert, 2009, 2012). Cryo-SEM techniques have been
98 applied in various approaches from cryo-fixation by plunge-freezing and lyophilization (Villena
99 et al., 2010), to freezing with liquid nitrogen and ethane followed by cryo-SEM imaging of the
100 frozen-hydrated biofilms (Wu et al., 2014; Beauvais et al., 2007). Wu et al. (2014) aptly point
101 out that different cryo-preparation methods give rise to markedly different biofilm
102 morphologies. Here we focus on ambient temperature SEM, and include cryo processing as
103 plunge-freezing with LN2, followed by freeze drying for conventional FESEM.

104 In this study, we share our observations on the ultrastructural component of biofilm
105 development (ECM and cellular) using conventional SEM, Field Emission SEM (FESEM) and VP-
106 SEM. We investigated the effect of processing techniques and reagents on the ultrastructure of
107 the cellular mycelium and ECM of two modes of biofilm growth of *A. fumigatus*: growth on a
108 solid substrate and growth in suspension at the liquid-air interface. Processing parameters
109 included: (1) time in primary aldehyde fixatives, (2) the inclusion of OsO_4 as a secondary
110 fixative, (3) final drying through CPD or HMDS and (4) hydrated structure analysis with VP-
111 SEM ~~(Table 1)~~ (5) inclusion of Ruthenium Red as contrasting agent for hydrated biofilms (6)
112 application of Ionic Liquid as alternative to conventional processing, and (6) Cryofixation and
113 lyophilization for FESEM analysis. We also (7) introduce Rutheniumtetroxide (RuO_4) as
114 alternative contrasting reagent to visualize hydrated biofilms using VP-SEM. We analyzed
115 samples with these varying parameters using a combination of two scanning electron

116 microscopes: a VP-SEM and a Field Emission SEM (FESEM). We provide our observations and
117 conclude with recommendations for *A. fumigatus* biofilm analysis by SEM.

118

119 *2. Material and Methods:*

120 *A.fumigatus* biofilms were grown in RPMI 1640 culture medium on 12 mm circular plastic
121 rotating bioreactor disks or as a floating biofilm mat close to the liquid-air interface in flasks.
122 For flask growth, a standardized *A. fumigatus* suspension was inoculated into 500ml
123 polystyrene tissue-culture flasks containing 100ml of RPMI-1640 medium (final concentration
124 10^5 conidia/ml) and incubated at 30°C for 96h. Biofilms on disks were formed by using a
125 modified in vitro model described previously (Ferreira JA et al., 2009, 2015). To form *A.*
126 *fumigatus* biofilms, sterile polystyrene disks (Biosurface Technologies, Bozeman, MT) were
127 placed in 12-well tissue culture plates (Corning Inc., MD, NY). Each well contained 3ml of fresh
128 RPMI-1640 medium (Lonza, Walkersville, MD) with 10^5 conidia/ml. Disks were incubated at
129 37°C for 16h with shaking at 70rpm, to allow the fungal cells to attach. Following the
130 attachment phase, disks were gently rinsed in sterile saline (Baxter Healthcare Corp.,
131 Cambridge, MA), transferred to new plates containing fresh RPMI-1640 medium, and incubated
132 for an additional 24h at 37°C with shaking at 100rpm.

133 2.1 For SEM processing, disks and biofilm mats were harvested and washed *in situ* twice
134 with 100ml of phosphate-buffered saline (PBS) to remove planktonic cells. Samples
135 were fixed in 4% paraformaldehyde (PFA) with 2% glutaraldehyde (GA) in 0.1M sodium
136 cacodylate buffer for varying incubation times (45mins – 24hrs, see Table 1). Samples
137 were then briefly rinsed in the same buffer before post-staining with 1% OsO_4 for
138 incubation times of 0 to 45mins (Table 1). For conventional SEM, OsO_4 -treated samples
139 were rinsed in water and gradually dehydrated in increasing concentrations of ethanol
140 (50-70, 90 100, 100%, 5mins each). Samples were then either dried with HMDS, or
141 critically point dried with liquid CO_2 using a Tousimis Autosamdri 815A and 15mins
142 purge time (Tousimis, Rockville, MD). Dried samples were sputter-coated (50Å, Au/Pd)
143 before imaging with a Hitachi 3400N SEM operated at 10kV under high vacuum, using

144 an Everhart-Thornley (ET) Secondary Electron (SE) detector, and a Zeiss Sigma FESEM
145 using InLens SE detection at 2kV (Carl Zeiss Microscopy Inc, Thornwood, NY).

146 2.2 For VP-SEM application, hydrated samples were visualized fully hydrated and either
147 unfixed, or fixed in aldehydes as described above for conventional SEM, followed by
148 post-fixation (45mins) in aqueous OsO_4 to enhance contrast of cellular material. Samples
149 were mounted in water on 10mm cup-shaped stubs custom-fitted for the Deben cold-
150 stage (Deben Ltd, Suffolk, UK), and temperature was gradually decreased during
151 evacuation, following a correlated graph for sublimation temperature and pressure of
152 water. VP-SEM was carried out with a Hitachi S-3400N VP-SEM (Hitachi High
153 Technologies, Pleasanton, CA) operated at 15kV and 50-60Pa, using Backscattered
154 Electron (BSE) detection and cold-stage (-25°C) control of hydration.

155 2.3 Staining with alternative heavy metals, Ruthenium Red: Disk grown *A.fumigatus* biofilms
156 were fixed in 4% PFA with 2% Glutaraldehyde for 45mins (see 2.1) and rinsed in buffer
157 (2x5mins), before (i) post-fixation in 0.01% Ruthenium Red for 1hr, or alternatively, (ii)
158 post-fixation in 0.01% Ruthenium Red (1hr) followed by incubation in OsO_4 (45mins).
159 Samples were rinsed in water (3x5mins) after incubation in each metal solution, and
160 visualized fully hydrated using VP-SEM as described above (2.1). Samples were kept in
161 water at 4˚C for a maximum of 24hrs before imaging.

162 2.4 Staining with Ruthenium Tetroxide (RuO_4): Disk grown *A.fumigatus* biofilms were fixed
163 in 4% PFA with 2% Glutaraldehyde for 45mins (see 2.1) and rinsed in buffer (2x5mins),
164 before post-fixation in 0.5% RuO_4 (1hr). All residual RuO_4 was removed by repeated
165 rinsing (3x5mins) in water, before visualizing biofilms fully hydrated using VP-SEM as
166 described above (2.1). Samples that were not visualized directly after staining were kept
167 in water at 4˚C and imaged within 24hrs.

168 2.5 Ionic Liquid (IL) treatment: Pellicles of flask grown *A. fumigatus* biofilms were fixed as
169 before in 4% PFA with 2% Glutaraldehyde, rinsed in 0.1M NaCacodylate Buffer (1x5min)
170 and, after removing most residual liquid, submerged in 100µl of either 5%, 10% or 20%
171 HILEM™ Ionic Liquid (Hitachi High Technologies, Pleasanton, CA) for 1hr at ambient
172 temperature. Samples were removed from IL and left to dry overnight on filter paper in

173 a desiccator before mounting and imaging (without Au/Pd sputter-coating) with a
174 Hitachi 3400N SEM operated at 5 and 10kV under high vacuum, using SE detection.
175 Based on the results obtained with *A. fumigatus* pellicles, disk grown *A. fumigatus*
176 biofilms were submerged in 10% IL (1hr) and dried and mounted similarly before SEM
177 imaging under high vacuum and without further conductive (Au/Pd) coating.

178 2.6 Cryofixation: Disk grown *A.fumigatus* biofilms were cryoprotected with 10% glycerol for
179 2hrs at 4C, plunge-frozen in liquid nitrogen and lyophilized before mounting and Au/Pd
180 sputter-coating for FESEM observation as described above (see 2.1).

181 *3. Results and Discussion:*

182 *A. fumigatus* biofilms form as a spongy mass of hyphae when grown at the liquid-air interface in
183 a glass flask. When cultured on a plastic disk submerged in liquid, the biofilm is a matted
184 network of hyphae closely associated with the solid substrate. The impact on biofilm structure
185 by various experimental parameters, summarized in Table 1, is discussed below.

186 3.1 SEM modality

187 3.1.1 VP-SEM (Fig.1): Inherent to VP-SEM is the poor SNR (Signal to Noise Ratio) due to gas
188 and moisture in the specimen chamber, and the ability of water to serve as an electron
189 dense sheet which may coat individual cells (hyphae) and obscure fine cellular features.
190 However, VP-SEM is ideally suited to visualize the native 3D architecture of hydrated
191 biofilms, which often collapses during dehydration for conventional SEM. It does not
192 typically employ drying and sputter-coating for conductivity and, thus, also enables
193 more rapid analysis. Stabilization of cells with aldehyde fixatives generally improved
194 structural preservation (Fig. 1), while post-fixation with OsO_4 (and other heavy metals,
195 see 3.3) enhanced the BSE signal (Fig. 1), which is the detector of choice for this EM
196 modality (in Hitachi S-3400N). Additionally, the lipid-binding properties of OsO_4
197 highlighted intra and extracellular lipids (often as droplets) in the fungal mycelium (Fig.
198 1 arrows). Therefore, using VP-SEM instead of high-vacuum SEM may better reveal
199 hydrated 3D architecture, but limits ultrastructural analysis of individual cells and ECM.

3.1.2 SEM and FESEM (Fig. 2&3): In our SEM analysis, a conventional Everhart-Thornley (ET)-SE detector was used, whereas our FESEM investigation applied an InLens SE detector. In both cultures (flask and disk grown), fungal hyphae occurred as flat filamentous structures, which were frequently connected with ECM material. ECM occurred either as stretched sheets (Fig. 2B & 3, white arrows) or fine, often reticulated fibers (Fig. 2B & 3, yellow arrows). Using high resolution FESEM, ECM was additionally characterized as an apparent rough, granular or vesicular coating (Fig. 3, red arrows) closely associated with hyphae. The nature of similar vesicles was suggested by our recent Transmission EM (TEM) analysis combined with solid-state NMR, which revealed isolated ECM from *A. fumigatus* to be vesicular as well as fibrous in nature (Reichhardt et al., 2015). Fungal biofilms, which apparently lacked ECM by gross inspection, thus revealed surprising quantities of ECM with high-efficiency InLens SE detection, which obtains high lateral resolution and edge contrast at low accelerating voltages. Post-fixation with OsO_4 generally enhanced SE and BSE detection in both SEM and FESEM analysis. Shorter periods in ~~both~~ aldehyde ~~and OsO_4~~ fixatives resulted in improved separation of fine structural features (Fig. 2 & 3), while longer fixation times caused a collapse of fungal mycelium and ECM fibers.

3.2 Processing for conventional (high-vacuum) SEM

3.2.1 Primary fixation: The high protein content of ECM, as reported by Reichhardt et al. (2015), results in efficient ultrastructural preservation of ECM by aldehydes. Primary fixation with aldehydes have been proven to provide the optimal ultrastructural preservation of living cells, in addition to preventing disruption during further processing steps (Bozzola and Russell, 1999). While GA provides superior stabilization of structure through its terminal aldehyde groups that crosslink amino groups in proteins, PFA has been included in low concentrations (up to 4%) to penetrate and preserve living cells more rapidly that the larger GA molecule (Karnovsky, 1965). By introducing this combination of PFA with GA, both rapid and more efficient stabilization of proteins is therefore accomplished. Since protein is a universal constituent of cells,

229 and has also been found to be a major component of the ECM of *A.fumigatus* biofilms
230 (Reichhardt et al., 2015), primary fixation with aldehydes (PFA and GA) stabilizes both
231 the cellular and extracellular component of *A. fumigatus* biofilms. One can envision that
232 aldehyde fixation cross-links soluble proteins to each other and to fixed membranes and
233 the cytoskeleton, as well as extracellular components in these biofilms. Its specificity is
234 not limited to proteins, and GA may also react with lipids, nucleic acids and
235 carbohydrates. Since the optimal concentration of primary fixatives that would
236 accomplish denaturation of proteins, without additional artefacts of autolysis and
237 extraction by different tonicities, have been proven to be below 4% PFA and 2-3% GA
238 (Bozolla and Russell, 1999; Dykstra, 1992; Coetzee and Van der Merwe, 1984, 1986;
239 Bone and Denton, 1971; Anniko and Lindquist, 1977), we used similar concentrations of
240 aldehydes for preservation of *A. fumigatus* biofilms. However, while extended incubation
241 times in aldehydes is generally accepted laboratory practice, in the case of *A.fumigatus*
242 biofilms, prolonged fixation (≥24hrs) often led to a collapse of fine features (Fig. 2A-
243 columns A, B) and a denser appearance of biofilm structure, probably due to increased
244 binding of associated and complex matrix materials, and physico-chemical factors in a
245 hydrated environment. By limiting the incubation time in primary fixatives to less than
246 an hour (45mins in this study) we found improved preservation of ECM ultrastructure –
247 which was the primary objective of our SEM investigations. This supports the
248 observation of Bozzolla and Russell (1999) that, due to the introduction of artefacts
249 during fixation, one always selects a particular fixation protocol for 'its ability to
250 preserve one ultrastuctural feature over another'.

251 3.2.2 Secondary fixation: OsO_4 is generally used as secondary fixative, both to stabilize
252 especially the lipid moieties of cells, and to act as 'stain' (contrasting agent) in being a
253 high molecular weight reagent. Its penetration rate is slower tan that of glutaraldehyde,
254 but since exposure for longer than 1.5hrs can lead to extraction of materials (Bozzola
255 and Russell, 1999), we similarly used short (less than 1hr) fixation times in OsO_4. In the
256 case *A. fumigatus* biofilms, post-fixation with OsO_4 generally improved ultrastructural
257 preservation, while enhancing SNR for both SE and BSE detection. The improved signal
258 from heavy metal staining also resulted in increased brightness and contrast in *A.*

259 *fumigatus* biofilms, which enabled improved characterization of cellular versus
260 extracellular biofilm components (Fig. 2B upper row, arrows). Since the phospholipid
261 component of cellular membranes, as well as the lipid component of ECM were better
262 preserved with addition of OsO_4, biofilm components also appeared less aggregated
263 after post-fixation with OsO_4 (Fig. 2A, rows 1&2).

264 3.2.3 CPD improved ultrastructural preservation of fine features, notably in ECM, while final
265 drying with HMDS often caused aggregation of hyphae and fine structures. *A. fumigatus*
266 biofilms that were dried with HMDS often appeared as aggregated hyphae connected by
267 sheets of ECM lacking fibrous ultrastructural features, and with collapsed vesicles. This
268 comparison illustrates the influence different drying methods can have on analysis.
269 HMDS provides a rapid low-cost alternative to CPD where sample format (or space and
270 funding) limits the use of CPD. However, results with *A. fumigatus* biofilms are superior
271 with CPD. CPD is designed to avoid perturbations from the surface tension of a
272 decreasing meniscus resulting from the evaporating dehydrating liquid by moving the
273 intermediary liquid (liquid CO_2) to its critical point (where the densities of liquid and gas
274 are identical) at which point the residual gas can be removed. Thus, the effect on final
275 structure should be carefully evaluated to determine drying–associated artifacts. At
276 lower magnification, this effect was most obvious in disk-grown biofilms (Fig.2A). At
277 higher magnification, drying artifacts were evident in ECM from both disk and flask
278 grown cultures. The effect is exacerbated when OsO_4 was excluded during fixation
279 (Fig.2B).
280

281 3.2.4 Disk grown biofilms formed a flatter, two-dimensional architecture than the spongy
282 three-dimensional structure of flask grown pellicles. Pellicles exhibited large pores and
283 channels surrounding an elaborate network of intertwined hyphae, which were often
284 partially compressed. This apparent vacuolization of hyphae may result from aging or
285 stress factors in the deeper biofilm layers (Lin and Austriaco, 2014, Flemming et al.,
286 2016). Hyphae on disks were closely associated with the plastic substrate, often
287 extended in parallel growth-patterns, and revealed more spherical ECM vesicles than in
288 the pellicles, where ECM was mostly visible as a network of fibrous material forming fine

289 sheets that stretch between hyphae. The appearance of ECM largely depended on the
290 fixation and drying techniques (3.2.1 – 3.2.3)
291
292 3.2.5 Fixing for prolonged times (at least 24 hrs), as typically done with biological samples,
293 caused a collapse of ECM and hyphae, resulting in poor preservation of biofilm
294 architecture, loss of 3D structure attributed to water loss through dehydration
295 techniques. Fixation for shortened times (less than 1hr) resulted in excellent
296 preservation of both cellular and extracellular components, and thereby improved
297 interpretation of ultrastructural features, i.e. mycelium/hyphae, ECM fibers and vesicles.
298 For *A. fumigatus* biofilms, such shortened fixation and post-fixation conditions proved to
299 be optimal for relevant interpretation of both hyphae and ECM ultrastructure (Fig. 2A, B
300 & Fig.3).

301

302 3.2.6 Cryofixation: Biofilms that were cryo-protected and prepared by plunge-freezing in LN2,
303 followed by lyophilization, showed remarkable preservation of both cellular (hyphae)
304 and ECM ultrastructure. Hyphae remained separated and non-compacted, while ECM
305 was present as fine reticulate fibers (Fig. 4). This technique requires minimal
306 preparation, while preliminary fixation with PFA and GA may also be included. Villena et
307 al. (2010) similarly observed differences in *Aspergillus niger* biofilm morphology when
308 applying cryo-fixation techniques to biofilms grown as pellicles versus substrate (cloth)-
309 attached films.

310

311 3.2.7 Ionic Liquid treatment: Ionic liquids are salts that exist in liquid state at room
312 temperature and do not evaporate under vacuum conditions in EM applications
313 (Arimoto et al., 2008; Asahi et al., 2015.). It provides both electrical conductivity and
314 hydration to biological specimens, and thereby enables electron microscopic
315 visualization of specimens without dehydration or sputter-coating with a conductive
316 metal. *A.fumigatus* pellicles (Fig.5A) and disk grown biofilms (Fig.5B) showed
317 remarkable conductivity and contrast, while retaining overall biofilm structure, when

318 treated with HILEM™ Ionic Liquid. Fixation with aldehydes may be included to stabilize
319 fine features, though was not a prerequisite to visualize biofilm structure, and did not
320 enhance image quality (Joubert & McDonald, 2016). Since *A.fumigatus* biofilms were
321 hydrated when treated with Ionic Liquids, the natural biofilm architecture was retained.
322 This was especially obvious at lower magnification (Fig.5A,B: 200x and 1,000x), while at
323 higher magnification hyphae appeared aggregated and closely associated, mostly due to
324 water and IL filling pores and channels between hyphae (Fig. 5A, B: 2,000-5,000x).
325 Fibrous ECM was not observed, since such fine structures will only be revealed after
326 extraction of water, as in conventional SEM. Residual IL may limit resolution of fine
327 surface features (Fig. 5B arrows), and at high magnification may result in artefacts such
328 as small bubbles appearing under the electron beam (data not shown). Biofilm
329 topography influenced sample conductivity, and this was observed especially where the
330 biofilm was forming a convoluted 3D structure that was lifted away from the substrate
331 during drying. Using lower accelerating voltages provided a suitable solution, though
332 while at the same time limiting resolution at higher magnification, which can only be
333 attained at higher accelerating voltages. Treating *A.fumigatus* pellicles with an
334 increasing series of IL concentrations (Fig. 5A), suggested 10% IL to be an optimal
335 concentration to enhance conductivity, limit charging artefacts, and prevent
336 accumulation of IL in porous areas. In the subsequent treatment of disk grown *A.*
337 *fumigatus* biofilms (Fig. 5B), only 10% IL was used, and samples imaged at high vacuum
338 without sputter-coating, and using ET-SE detection. Draining off all residual IL is
339 important where either porous areas or fine features need to be resolved. Given the
340 rapid preparation, needing very few materials and no ancillary equipment, IL provides a
341 valuable tool to explore biofilms in their natural (hydrated) state under high vacuum
342 and using SE detection (Sakaue et al., 2014, Joubert and McDonald, 2016).
343
344 3.3 Contrasting for VP-SEM (Fig. 1 & 6): Since VP-SEM systems mostly use BSE Detection for
345 visualization, with the signal consequently related to the atomic weight of the specimen,
346 inclusion of heavy metals during processing can provide both a stabilization (fixation)
347 aspect in addition to improving contrast and resolution. OsO_4 has been proven throughout
348 the history of EM to provide excellent fixation in cells (Porter and Kallman, 1953). It

349 oxidizes double bonds in unsaturated fatty acids and is reduced to an electron-dense
350 product at the reduction site (Bozzola and Russell 1999). Contrasting with OsO_4 therefore
351 provides a specific contrasting agent for lipid-containing areas in the cell, though it has
352 been described (Porter and Kallmann, Bozzola and Russell) to react with various other cell
353 components, including proteins – and also acts as a mordant, in later combining with
354 stains and contrasting agents. Here we observed enhanced contrasting of lipid droplets
355 inside hyphae, in addition to improved resolution of cell membranes and biofilm structure
356 (Fig. 1& 6).
357
358 Ruthenium Red has similarly been used over decades (Reimann 1961, Dierichs 1979, Luft
359 1971) as a cell wall stain in electron microscopy, and not only binds with phospholipid
360 membranes, but also associates with Ca2+-binding proteins. Both specific and non-specific
361 adsorption models have been proposed (Voelker and Smejtek, 1996). Chemical reactions
362 between Ruthenium Red and OsO_4 also apparently bind these heavy metals to cell
363 surfaces, where it provides contrast enhancement (Dierichs 1979). We applied Ruthenium
364 Red both as single reagent, and in combination with OsO_4 (see 2.3). As a single stain,
365 contrast was enhanced in hyphae as well as ECM (Fig. 6 top row, short arrows), probably
366 due to the ability of Ruthenium Red to bind to both lipid and protein components of the
367 cellular and extracellular biofilm components. In combination with OsO_4, the lipid
368 component of hyphae was more strongly enhanced, similar to staining with OsO_4 alone
369 (Fig.6, second row, long arrows). Both forms of Ruthenium Red (with and without OsO_4)
370 provides a valuable contrasting alternative to biofilms, and since Ruthenium Red is much
371 less toxic than OsO_4 , this reagent can be used with great success in VP-SEM applications.
372
373 We finally applied RuO_4 as contrasting reagent in hydrated and aldehyde-fixed *A.*
374 *fumigatus* biofilms. RuO_4 is closely related to OsO_4 , fixes membranes and polymeric
375 materials, and has been described as a 'far more vigorous' oxidant than OsO_4 (Trent et al.,
376 1983). According to Gaylarde and Sarkany (1968) RuO_4 also reacts more strongly with
377 more polar lipids, as well as proteins, glycogen and monosachharides. Our results with VP-
378 SEM visualization of *A. fumigatus* biofilms illustrated this heavy-metal reagent as an
379 excellent contrasting agent for both cellular and ECM components of the biofilm (Fig.6,

380 third row). Hyphae were well preserved, while resolution was enhanced by the gain in
381 contrast. ECM showed similar enhanced contrast, and the fibrous ultrastructure was
382 resolved both on and between hyphae (Fig. 6 short arrows) - an aspect that was
383 unattainable when OsO4 was included as contrasting agent. Given the protein and lipid
384 moieties of *A. fumigatus* biofilms (Reichhardt et al., 2015) we introduce this heavy-metal
385 reagent as a valuable fixative and contrasting agent in fungal biofilm studies.

386 Our results suggest that consistent high-resolution ultrastructural SEM analysis of cellular
387 features and ECM of *A. fumigatus* biofilms can be achieved using a relatively short fixation time
388 and including OsO_4 post-fixation, followed by CPD. It is also evident, even at low magnifications,
389 (Fig. 2A) that the combination of extended fixation times, a lack of OsO_4 combined, and HMDS
390 drying yield the poorest preservation of ultrastructure in both disk and flask cultures.

391 In Table 2 we compare the described processing techniques to suggest a practical workflow in
392 the laboratory, and highlight the time, equipment and expertise needed for each procedure.

393

394 *Conclusions:*

395 In-depth analysis of compositional, structural and functional aspects of *A. fumigatus* is needed
396 to identify new antifungal targets (Kaur & Singh, 2014) and can ultimately be leveraged to
397 design therapeutic agents for the control of *A. fumigatus* biofilm-associated infection and
398 contamination. Electron microscopy is unparalleled in its ability to visualize microbial biofilms.
399 This visualization is crucial in connecting differences in biofilm composition with function.
400 However, variations in sample preparation protocols, microscope selection, and acquisition
401 parameters can influence the observed ultrastructure in biological samples, particularly
402 biofilms.

403 From the broadest perspective, VP-SEM is a superb modality where hydrated 3D biofilm
404 structure is of greater importance than ultrastructural surface features of individual cells
405 (hyphae in *A. fumigatus*). However, water is electron dense. Trapped water in hydrated biofilms
406 can cause closely associated hyphae to appear as thick strands, limiting resolution and even
407 preventing distinction between hyphal strands and ECM. Thus, where ultrastructural features

408 of cellular and ECM components are desired, high-resolution SEM and FESEM techniques using
409 SE detection are superior.

410 For each imaging modality (VP-SEM with BSE detection, conventional SEM with ET-SE
411 detection, and FESEM with InLens SE detection), we observed that the maintenance of biofilm
412 ultrastructure during SEM analysis also depended on the sample fixation parameters (fixative
413 and fixing time) and sample drying method (CPD vs. HDMS). Optimal parameters also differed
414 for pellicles (with biofilms formed at the air-liquid interface) and biofilms attached to plastic.
415 Thus, sample preparation parameters should be optimized for any new biofilm sample. Our
416 general recommendations for SEM visualization of *A. fumigatus* biofilms include the following:
417 (1) A short primary fixation time of up to 1 hr is ideal for sample preparation, where longer
418 fixing times, e.g. 24 hours, compromise the integrity of the biofilm architecture. (2) Post-
419 fixation with OsO_4 yields improved contrast and visualization of cellular versus extracellular
420 regions, attributed to the enhanced staining of lipids within cells and as extracellular
421 component of ECM. Due to the complex and varying nature of ECM, other heavy-metal reagents
422 such as Ruthenium Red and RuO4 may provide both a wider spectrum and more specific
423 contrasting of biofilm components (3) Sample drying using CPD is superior to HDMS and
424 improves the ultrastructural preservation of fine features in the ECM. (4) Specimen preparation
425 with cryo-fixation and lyophilization provides a valuable and rapid alternative to conventional
426 chemical fixation and drying. In summary, our analysis presented here emphasizes the
427 complexities in visualizing the attached lifestyle of microbial communities and provides our
428 results and recommendations for visualizing biofilms formed by *A. fumigatus*.

429 *Acknowledgements*

430 These studies were partially supported (D.A.S.) by a grant from the Child Health Research
431 Institute, Stanford Transdisciplinary Initiatives Program, and a gift from John Flatley. L-M.J. was
432 partially supported by the Beckman Foundation and a Technology Innovation mini-grant and
433 J.A.F. by a grant from the Brazilian National Council for Scientific and Technological
434 Development (CNPq). The material is based in part upon work supported (L.C.) by the National
435 Science Foundation CAREER Award (1453247). Hitachi High Technologies is thanked for
436 providing HILEM™ IL.

437 *References:*

438 Alhede M., Qvortrup K., Liebrechts R., Høiby N., Givskov M., Bjarnsholt T. (2012). Combination
439 of microscopic techniques reveals a comprehensive visual impression of biofilm structure and
440 composition. FEMS Immunol. Med.Microbiol. 65: 335-342.

441 Anniko, M. and Lundquist, P-G. (1977). The influence of different fixatives and osmolality on the
442 ultrastructure of the cochlear neuroepithelium. Arch Otorhinolaryngol 218:67-78.
443 doi:10.1007/BF00469735

444 Arimoto A., Sugimura M., Kageyama H., Torimoto T., Kuwabata S. (2008). Development of new
445 techniques for scanning electron microscope observation using ionic liquid. Electrochim Acta 53
446 (21): 6228-6234. Doi:10.1016/j.electacta.2008.01.001

447 Asahi Y., Muira J., Tsuda T., et al. (2015). Simple observation of *Streptococcus mutans* biofilm by
448 scanning electron microscopy using ionic liquids. AMB Express 5 (1): 6-14.

449 Beauvais A., Schmidt C., Guadagnini S., Roux P., Perret E., Henry C., Paris S., Mallet A., Prevost
450 M.C., Latge J.P. (2007). An extracellular matrix glues together the aerial-grown hyphae of
451 *Aspergillus fumigatus*. Cell Microbiol 9:1588–1600. doi:.10.1111/j.1462-5822.2007.00895.x.

452 Beauvais A., Loussert C., Prevost MC., Verstrepen K., Latge JP. (2009). Characterization of a
453 biofilm-like extracellular matrix in FLO1-expressing *Saccharomyces cerevisiae* cells. FEMS Yeast
454 Res 9:411–419. doi:.10.1111/j.1567-1364.2009.00482.x.

455 Beauvais A., Fontaine T., Aimanianda V., Latge J.P. (2014). *Aspergillus* cell wall and biofilm.
456 Mycopathologia 178:371–377. doi:.10.1007/s11046-014-9766-0.

457 Bone, Q. and Denton, E.J. (1971). The osmotic effects of electron microscope fixatives. JCB
458 49(3): 571-574. DOI: 10.1083/jcb.49.3.571

459 Bozzola J.J. and Russell L.D. (1999). Electron Microscopy Principles and Techniques for
460 Biologists. 2nd Ed. Jones and Bartlett Publishers, Sudbury, MA.

461 Bray D.F., Bagu J. and Koegler P. (1993). Comparison of hexamethyldisilazane (HMDS), Peldri II,
462 and critical-point drying methods for scanning electron microscopy of biological specimens.
463 Microsc Res Tech 26:489-495.

464 Chotirmall S.H., Mirkovic B., Lavelle G.M., McElvaney N.G. (2014). Immunoevasive *Aspergillus*
465 virulence factors. Mycopathologia 178: 363-370.
466
467 Coetzee, J. and Van der Merwe, C.F. (1984). Extraction of substances during glutaraldehyde
468 fixation of plant cells. Journal of Microscopy, 135: 147–158. doi:10.1111/j.1365-
469 2818.1984.tb00515.x

470 Coetzee, J. and Van der Merwe, C.F. (1986). The osmotic effect of glutaraldehyde-bawed
471 fixatives on plant storage tissue. Jnl. Microscopy 141: 111-118. DOI: 10.1111/j.1365-
472 2818.1986.tb02705.x

473 Costerton J.W., Lewandowski Z., Caldwell D.E., Korber D.R., Lappin-Scott H.M. (1995). Microbial
474 Biofims. Annu Rev Microbiol. 49: 711-745.

475 De Vrankrijker A.M., van der Ent C.K., van Berkhout F.T., Stellato R.K., Willems R.K., Bonten M.J.,
476 Wolfs T.F. (2011). *Aspergillus fumigatus* colonization in cystic fibrosis: implications for lung
477 function? Clin Microbiol Infect. 17(9):1381-1386. doi: 10.1111/j.1469-0691.2010.03429.x.

478 Dierichs R. (1979). Ruthenium red as a stain for electron microscopy. Some new aspects of its
479 application and mode of action. Histochemistry 64(2): 171-187.
480
481 Donlan R.M. (2002). Biofilms: Microbial Life on Surfaces. Emerging infectious Diseases 8(9):
482 881-890. doi: 10.3201/eid0809.020063.
483
484 Ferreira J.A., Carr J.H., Starling C.E., de Resende M.A., Donlan R.M. (2009). Biofilm formation and
485 effect of caspofungin on biofilm structure of *Candida* species bloodstream isolates. Antimicrob
486 Agents Chemother. 53:4377-4384. doi: 10.1128/AAC.00316-09 PMID: 19546368.

487 Flemming H.C., Neu T.R., Wozniak D.J. (2007). The EPS matrix: the "house of biofilm cells". J
488 Bacteriol 189: 7945–7947.
489
490 Flemming H-C., Wingender J., Szewzyk U., Steinberg P., Rice S.A., Kjelleberg S. (2016). Biofilms:
491 an emergent form of bacterial life. Nature Rev. Microbiol. 14: 563-575.
492 doi:10.1038/nrmicro.2016.94
493
494 Fox E.P. and Nobile CJ. (2012). A sticky situation: untangling the transcriptional network
495 controlling biofilm development in *Candida albicans*. Transcription 3: 315-322.
496
497 Gaylarde P, and Sarkany I. (1968). Ruthenium tetroxide for fixing and staining cytoplasmic
498 membranes. Science 161 (3846): 1157-1158. DOI: 10.1126/science.161.3846.1157
499
500 Hayat M.A. (2000). Principles and Techniques of Electron Microcopy, Biological Applications.
501 4th Ed. Cambridge University Press, Cambridge, UK.
502
503 Joubert L-M. (2009). Visualization of Hydrogels with Variable Pressure SEM. Microscopy and
504 Microanalysis, Volume 15, Supplement S2, July 2009, pp 1308-1309.
505
506 Joubert L-M. (2012). VP-SEM: Unsung hero of SEM imaging. Imaging and Microscopy, Dec 2012,
507 p.1-5 http://www.imaging-git.com/
508
509 Joubert L-M., Ferreira J.A.G., Stevens D.A., Cegelski L. (2015). *Aspergillus fumigatus* biofilms
510 SEM: effect of processing techniques. Microsc. Microanal. 21(S3):935-936. DOI:
511 10.1017/S1431927615005474.

512 Joubert L-M. and McDonald K. (2016). SEM Visualization of Biological Samples using Hitachi
513 Ionic Liquid HILEM IL 1000: a Comparative Study. Microsc. Microanal. 22(S3), pp. 1170–1171.
514 doi: 10.1017/S1431927616006693.
515
516 Kaur S. and Singh S. (2014). Biofilm formation by *Aspergillus fumigatus*. Med Mycol. 52(1): 2-9.

517 Kojic E.M. and Darouiche R.O. (2004). *Candida* infections of medical devices. Clin Microbiol Rev
518 17: 255-267.

519 Lappin-Scott H.S., Burton S., Stoodley P. (2014). Revealing a world of biofilms — the pioneering
520 research of Bill Costerton. Nature Rev. Microbiol. 12: 781-787.

521 Luft J.H. (1971). Ruthenium Red and violet. I. Chemistry, purification, methods of use for electron
522 microscopy and mechanism of action Anat. Red. 171:347-368.

523 Manavuthu E.K., Vager D.L., Vazquez J.A. (2014). Development and antimicrobial susceptibility
524 studies of in vitro monomicrobial and polymicrobial biofilm models with *Aspergillus fumigatus*
525 and *Pseudomonas arruginosa*. BMC Microbiol 14:53.

526 Mowat E., Butcher J., Lang S., Williams C., Ramage G. (2007). Development of a simple model for
527 studying the effects of antifungal agents on multicellular communities of *Aspergillus fumigatus*. J
528 Med Microbiol 56:1205–1212. doi:.10.1099/jmm.0.47247-0.

529 Muller F.M,, Seidler M., Beauvais A. (2011). *Aspergillus fumigatus* biofilms in the clinical setting.
530 Med. Mycol. 49: Suppl 1, S96-S100. doi: 10.3109/13693786.2010.502190. Epub 2011.

531 Nobile C.J. and Johnson A. (2015). *Candida albicans* biofilms and human disease. Annu Rev
532 Microbiol 69: 71-92.
533
534 Polke M., Hube B., Jacobsen I.D. (2015). *Candida* survival strategies. Adv Appl Microbiol 91:
535 139-235.
536
537 Porter K.R. and Kallman F. (1953). The properties and effects of osmium tetroxide as a tissue
538 fixative with special reference to its use for electron microscopy. Exp Cell Res 4(1): 127-141.
539
540 Priester J.H., Horst A.M., Van de Werfhorst L.C., Saleta J.L., Mertes L.A., Holden P.A. (2007).
541 Enhanced visualization of microbial biofilms by staining and environmental scanning electron
542 microscopy. J Microbiol Methods 68: 577–587.

543 Reichhardt C., Ferreira J.AG., Joubert L-M., Clemons K.V., Stevens D.A., Cegelski L. (2015).
544 Analysis of the *Aspergillus fumigatus* Biofilm Extracellular Matrix by Solid-State Nuclear
545 Magnetic Resonance Spectroscopy. Eukaryot Cell. 14(11):1064-72. doi: 10.1128/EC.00050-15.
546 Epub 2015 Jul 10.

547 Reichhardt, C., Stevens, D.A., Cegelski, L. (2016) Fungal biofilm composition and opportunities
548 in drug discovery. Future Medicinal Chem., in press.

549 Reimann B. (1961). Zur Verwendbarkeit von Rutheniumrot als elektronmikroskopisches
550 Kontrastierungsmittel. Mikroskopie 16:224-226.

551 Sakaue, M., Shiono, M., Konomi, M., Tomizawa, J., Nakazawa, E., Kawai, K., Kuwabata, S. (2014)
552 New preparation Methods using ionic Liquid for Fast and Reliable SEM Observation of
553 Biological Specimens. Microsc. Microanal. 20(S3): 1012-2013. doi:
554 10.1017/S1431927614006783

555 Santos, A.L.S. (2015). Biofilm: A robust and efficient barrier to antifungal chemotherapy. J.
556 Antimicro 1: e101. doi:10.4172/Antimicro.1000e101.

557 Speirs J.J., Van der Ent C.K. and Beekman J.M. (2012). Effects of *Aspergillus fumigatus*
558 colonization on lung function in cystic fibrosis. Curr Opin Pulm Med. 18:632-638.

559 Trent J.S., Scheinbeim J.I., Couchman P.R. (1983). Ruthenium Tetraoxide Staining of Polymers
560 for Electron Microscopy. Macromolecule 16: 589-598.

561 Villena, G.K., Fujikawa, T., Tsuyuma, S., Gutierrez-Correa, M. (2010). Structural analysis of
562 biofilms and pellets of Aspergillus niger by confocal laser scanning microscopy and cryo
563 scanning electron microscopy. Bioresour. Technol. 101: 1920-1926.

564 Voelker D. and Smejtek, P. (1996.) Adsorption of Ruthenium Red to Phospholipid Membranes.
565 Biophys J. 70:818-830.

566 Weber K., Delben J., Bromage T.G., Duarte S. (2014). Comparison for SEM and VPSEM imaging
567 techniques with respect to Streptococcus mutants biofilm topography. FEMS Microbiol Lett.
568 350:175-179.

569 Weimer P.J., Price N.P., Kroukamp O., Joubert L.M., Wolfaardt, G.M., Van Zyl W.H. (2006). Studies
570 of the extracellular glycocalyx of the anaerobic cellulolytic bacterium *Ruminococcus albus* 7.
571 Appl Environ Microbiol 72: 7559–7566.
572
573 Xiao J., Klein M.I., Falsetta M.L., et al. (2012). The exopolysaccharide matrix modulates the
574 interaction between 3D architecture and virulence of a mixed-species oral biofilm. PLoS Pathog
575 8(4): e1002623. doi:10.1371/journal.ppat.1002623.
576
577 Yousif A., Jamal M.A., Raad I. (2015). Biofilm-based central line-associated bloodstream
578 infections. Adv Exp Med Biol 830: 157-179.
579
580

BIOFILM CULTURE (x2): FLASK versus DISK							
2%GA + 4%PFA, postfix 1%OsO_4				2%GA + 4% PFA (no OsO_4)			
24hrs fix		45min fix		24hrs fix		45min fix	
CPD	HMDS	CPD	HMDS	CPD	HMDS	CPD	HMDS
Hydrated: VP-SEM (60Pa)				Hydrated: VP-SEM (60Pa)			

581

582 TABLE 1: Summary of fixation and drying parameters used to process *A. fumigatus* biofilms for
583 SEM visualization.

584

585

586

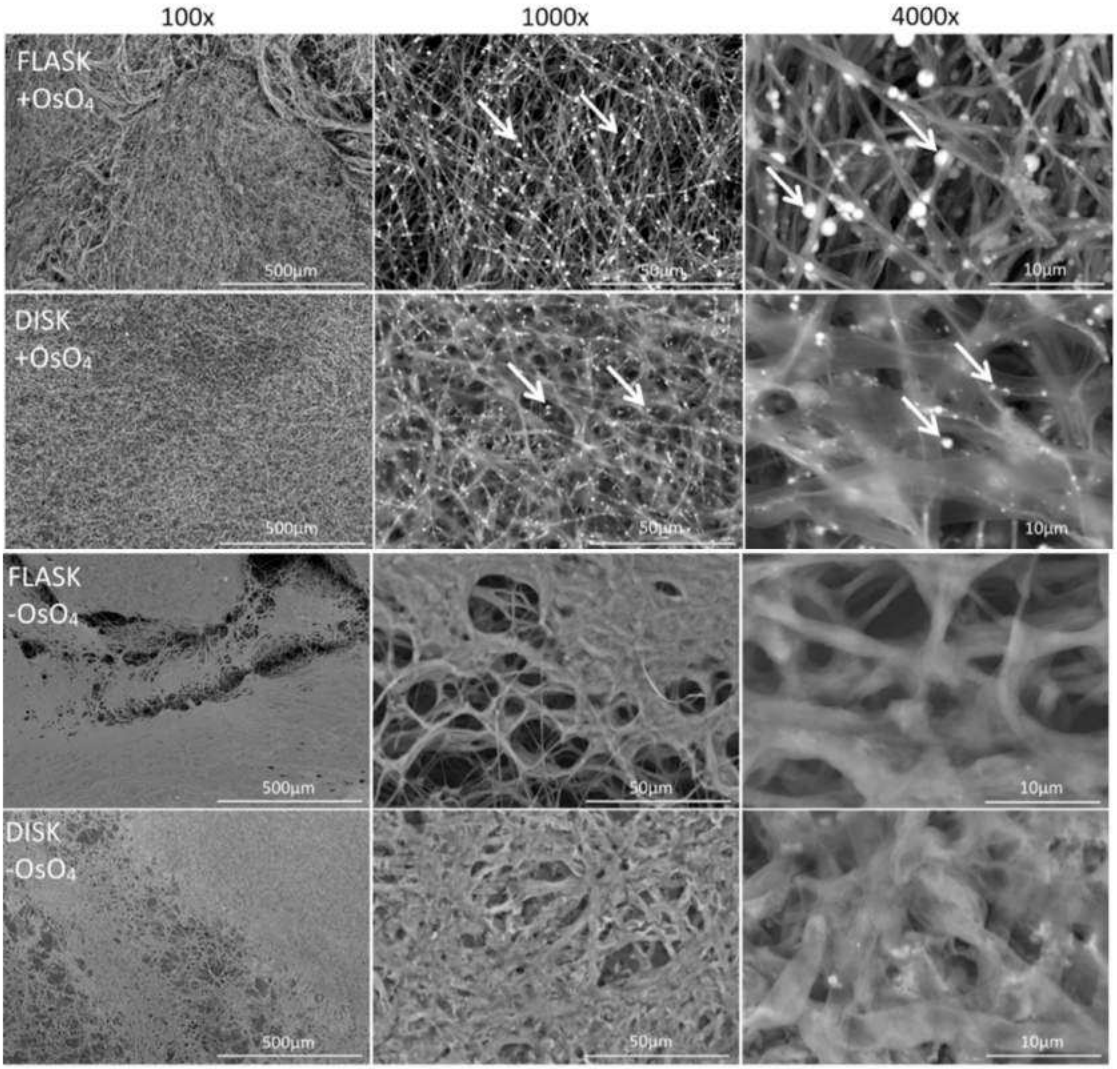

587

588

589 FIGURE 1: Flask vs. disk-grown: VP-SEM of hydrated and unfixed *A.fumigatus* biofilms including
590 OsO_4 (two upper rows) and excluding OsO_4 (two lower rows) post-fixation. OsO_4-enhanced
591 lipids are indicated by arrows

592

593

594

595

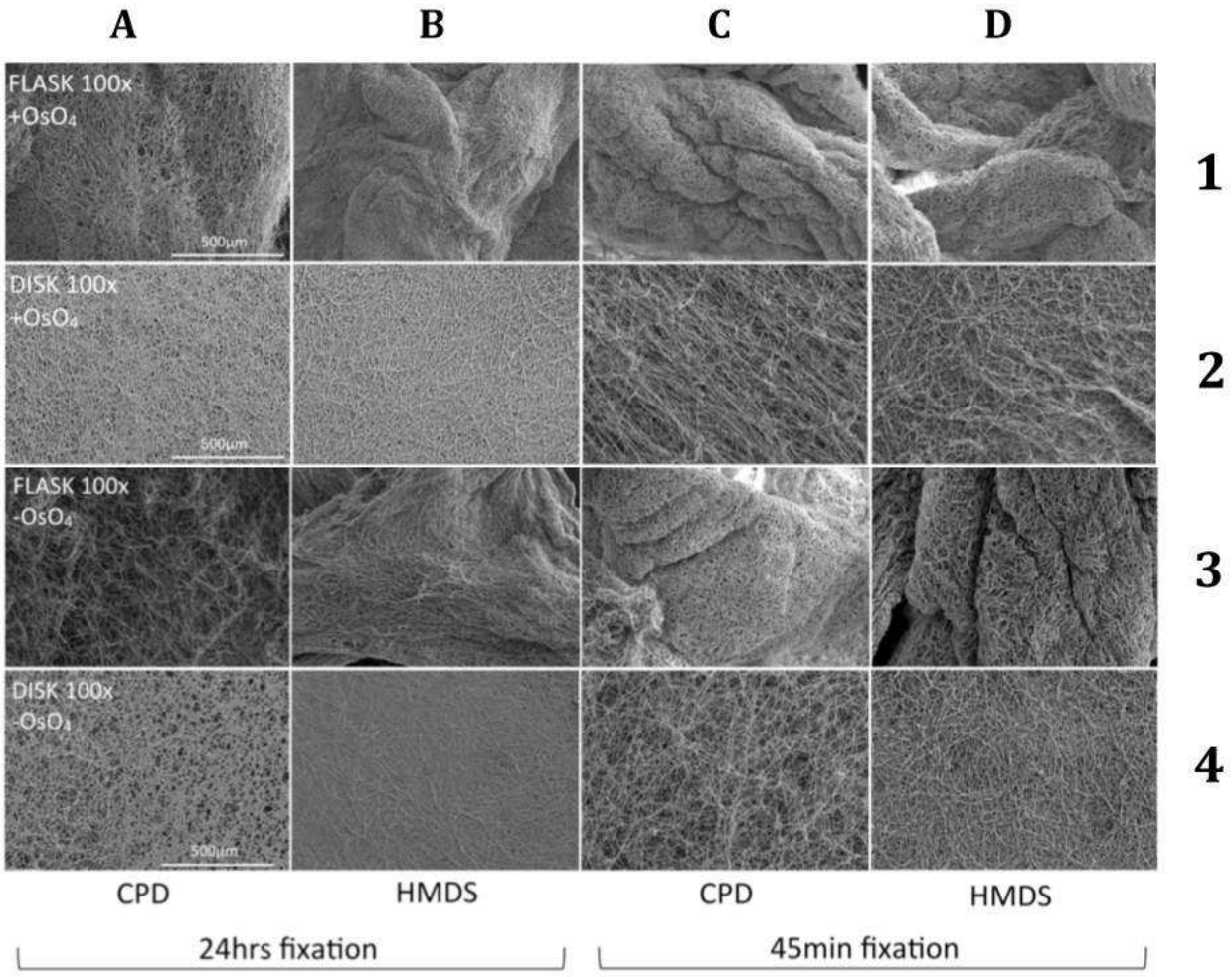

FIGURE 2A: Flask vs. disk-grown *A.fumigatus* biofilms, CPD vs. HMDS dried, 24hrs vs. 45mins fixation, with OsO_4 (upper rows) and without OsO_4 (lower rows). Prolonged fixation (columns A & B) result in denser appearance of biofilm through collapsed fine features. Addition of OsO_4 similarly led to less aggregated biofilm architecture (Rows 1 & 2). A combination of OsO_4 and CPD treatment therefore resulted in optimal biofilm structure (C2: Column C, Row 2)

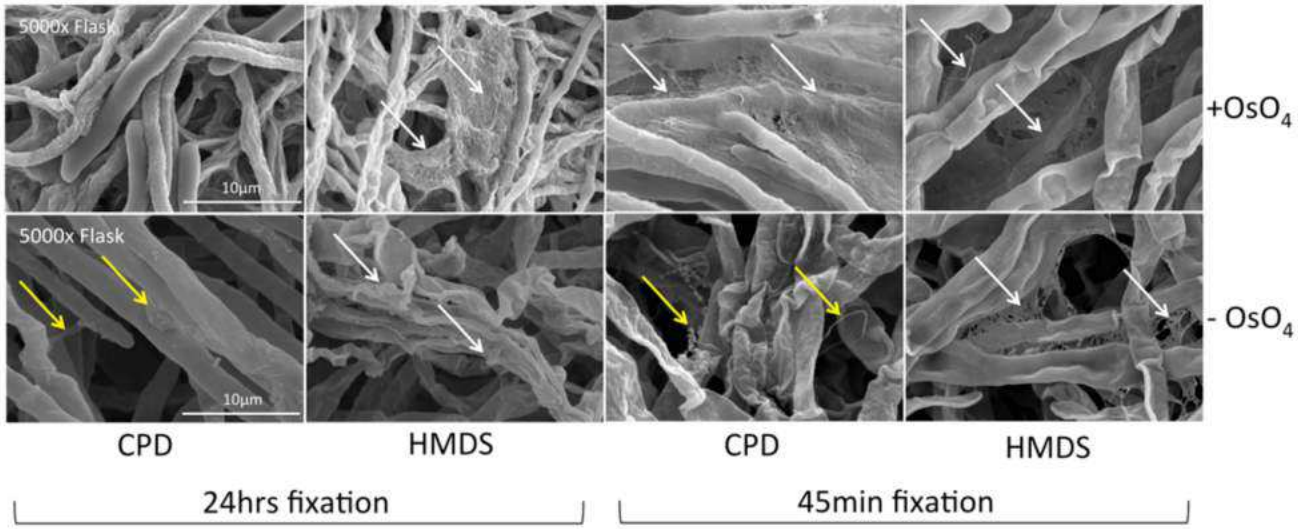

FIGURE 2B High magnification (5,000x) micrographs of flask-grown *A. fumigatus* biofilms illustrating hyphal and ECM features: CPD vs. HMDS dried; 24hrs vs. 45mins fixation; +/- OsO_4. Post-fixation with OsO_4 led to improved SNR and contrast-enhanced resolution of cellular and extracellular biofilm components. White arrows: ECM occurred either as stretched sheets. Yellow arrows: ECM occurring as fine or reticulated fiber

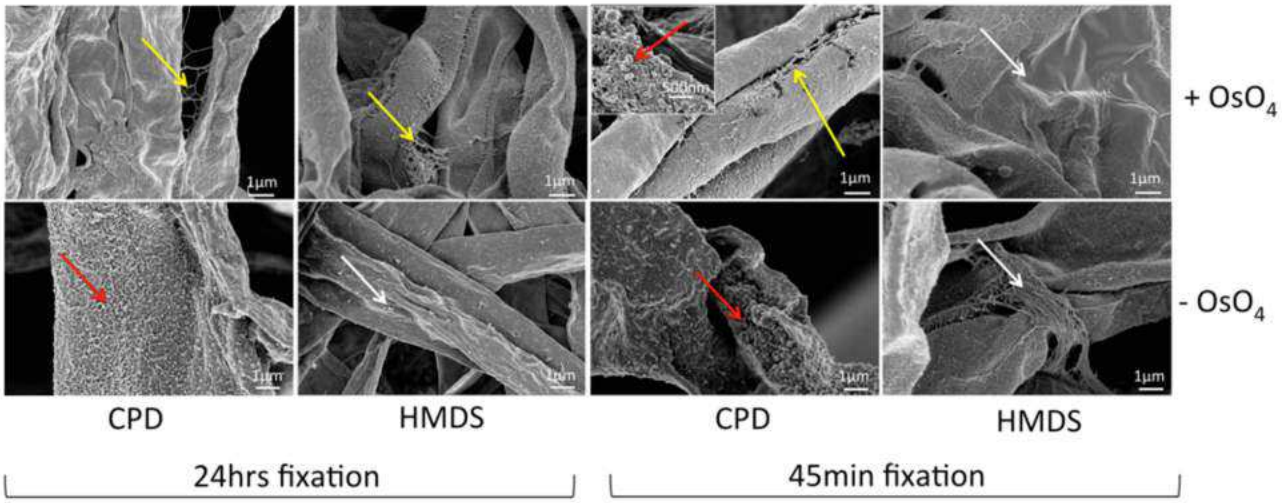

FIGURE 3: FESEM of *A. fumigatus* biofilms, with and without OsO_4 postfixation. ECM features are characterized with high definition InLens SE detection at 10,000x magnification. White arrows = stretched sheet of ECM; yellow arrows = fine or reticulate fibers of ECM; red arrows = ECM occurring as a rough, granular or vesicular coating, closely associated with hyphae. Inset shows ECM as a vesicular coating at 20,000x magnification.

632 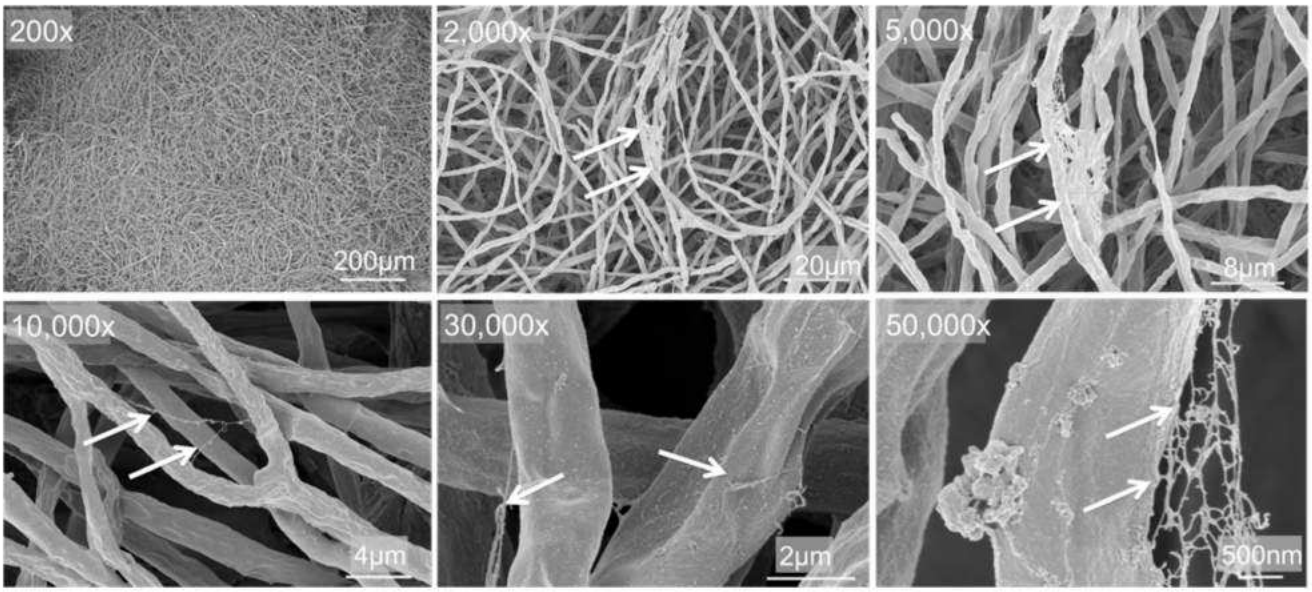

633 FIGURE 4: Cryofixation of disk grown *A. fumigatus* biofilms reveal well-preserved hyphae and
634 ECM (arrows) in a non-collapsed 3D biofilm architecture.

635

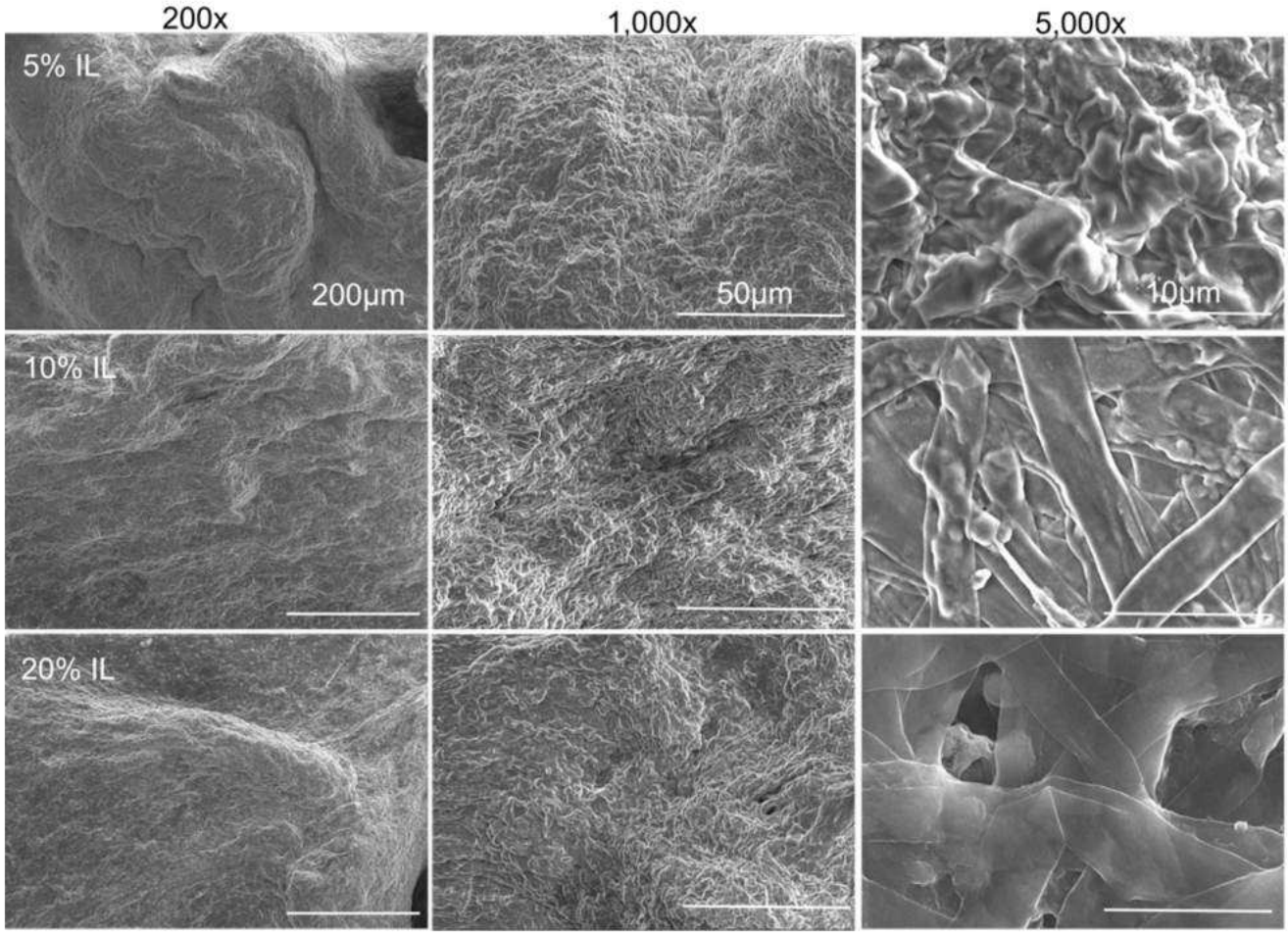

FIGURE 5A: *A. fumigatus* biofilm pellicles treated with 5%, 10% and 20% HILEM Ionic Liquid, and imaged at increasing magnification (200x, 1,000 x, 5,000x) at 5kV, using ET-SE detection and without Au/Pd sputter-coating. Lower concentrations (5%) of IL exhibited more artifacts of beam interference, while biofilm topography, and associated charging artefacts, played a more important role than IL concentration in final image quality and resolution.

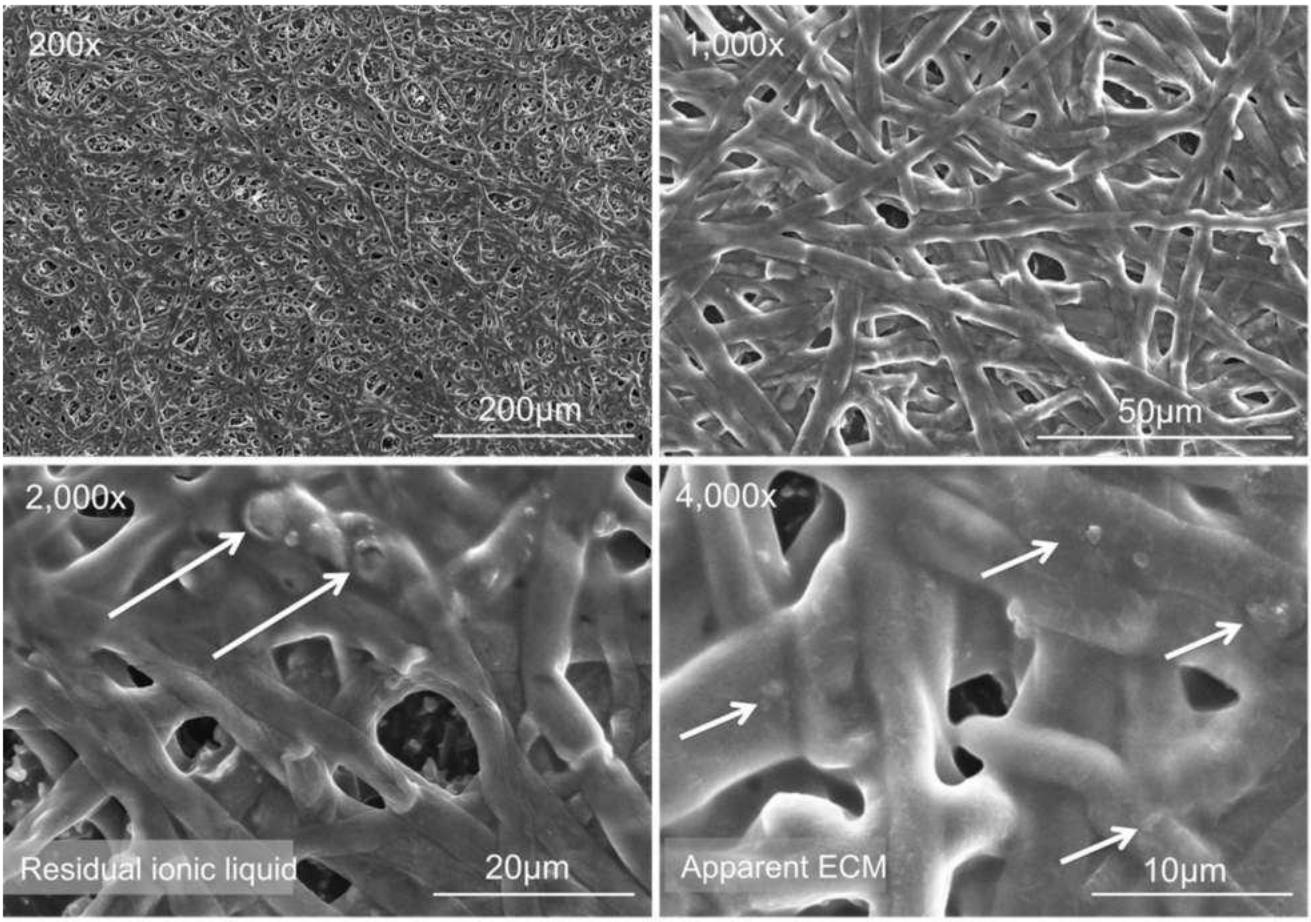

FIGURE 5B: Disk grown *A.fumigatus* biofilms treated with 10% HILEM Ionic Liquid, and imaged at increasing magnification (200x, 1,000 x, 2,000x and 5,000x) at 5kV, using ET-SE detection and without Au/Pd sputter-coating. Hydrated biofilm architecture was retained, while fine features were often hidden by residual IL (2,000: arrows). After thorough draining of IL, apparent ECM could still be observed at higher magnification (4,000x: arrows)

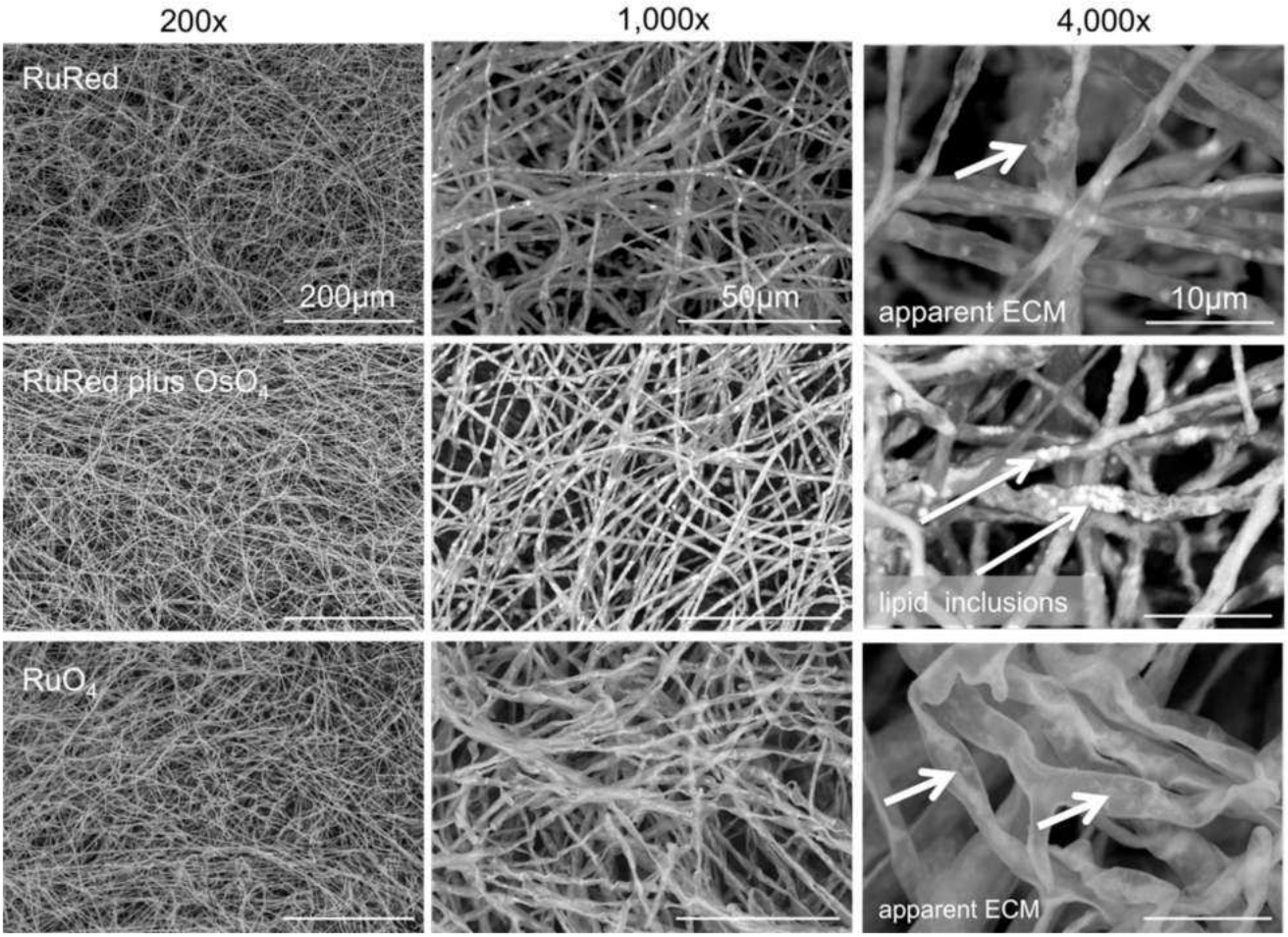

FIGURE 6: VP-SEM of fully hydrated disk grown *A.fumigatus* biofilms after post-fixation with various heavy metals show enhanced contrasting of hyphae, ECM (short arrows) and included lipids (long arrows). Ruthenium Red (top row) and RuO_4 (third row) show improved fixation and resolution of ECM, while addition of OsO_4 (second row) highlight lipid inclusions over ECM features.